

Incommensurate magnetic response in cuprate perovskites

A. Sherman

Institute of Physics, University of Tartu, Riia 142, 51014 Tartu, Estonia

Abstract

The incommensurate magnetic response of the normal-state cuprate perovskites is interpreted based on Mori's memory function approach and the t - J model of Cu-O planes. In agreement with experiment the calculated dispersion of the susceptibility maxima has the shape of two parabolas with upward and downward branches which converge at the antiferromagnetic wave vector. The maxima are located at $(\frac{1}{2}, \frac{1}{2} \pm \delta)$, $(\frac{1}{2} \pm \delta, \frac{1}{2})$ and at $(\frac{1}{2} \pm \delta, \frac{1}{2} \pm \delta)$, $(\frac{1}{2} \pm \delta, \frac{1}{2} \mp \delta)$ in the lower and upper parabolas, respectively. The upper parabola reflects the dispersion of magnetic excitations of the localized Cu spins, while the lower parabola arises due to a dip in the spin-excitation damping at the antiferromagnetic wave vector. For moderate doping this dip stems from the weakness of the interaction between the spin excitations and holes near the hot spots.

Key words: Cuprate superconductors, Magnetic properties, t - J model

PACS: 74.72.-h, 74.25.Ha, 71.10.Fd

One of the most interesting features of the inelastic neutron scattering in lanthanum cuprates is that for hole concentrations $x \gtrsim 0.04$, low temperatures and small energy transfers the scattering is peaked at incommensurate momenta $(\frac{1}{2}, \frac{1}{2} \pm \delta)$, $(\frac{1}{2} \pm \delta, \frac{1}{2})$ in the reciprocal lattice units $2\pi/a$ with the lattice period a [1]. For $x \lesssim 0.12$ the incommensurability parameter δ is approximately equal to x and saturates for larger x [2]. The incommensurate response was observed both below and above T_c [3]. Recently the analogous low-frequency incommensurability was observed in $\text{YBa}_2\text{Cu}_3\text{O}_{7-y}$ [4]. This gives grounds to suppose that the incommensurability is a common feature of cuprate perovskites which does not depend on subtle details of the energy structure. However, for larger frequencies the susceptibility differs essentially in these two types of cuprates. In the underdoped $\text{YBa}_2\text{Cu}_3\text{O}_{7-y}$ both below and above T_c a maximum was observed at frequencies $\omega_r = 25 - 40$ meV

Email address: alexei@fi.tartu.ee (A. Sherman).

[5]. For this frequency the magnetic response is sharply peaked at the antiferromagnetic wave vector $\mathbf{Q} = (\frac{1}{2}, \frac{1}{2})$. Contrastingly, no maximum at ω_r was observed in lanthanum cuprates [6]. For even larger frequencies the magnetic response becomes again incommensurate in both types of cuprates with peaks located at $(\frac{1}{2} \pm \delta, \frac{1}{2} \pm \delta)$, $(\frac{1}{2} \pm \delta, \frac{1}{2} \mp \delta)$ [5,7,8]. The dispersion of the maxima in the susceptibility resembles two parabolas with upward and downward branches which converge at $\mathbf{k} = \mathbf{Q}$ and $\omega \approx \omega_r$ [8].

The nature of the magnetic incommensurability is the subject of active discussion nowadays. The most frequently used approaches for its explanation are based on the picture of itinerant electrons with the susceptibility calculated in the random phase approximation [9] and on the stripe domain picture [8,10]. In the former approach the low-frequency incommensurability is connected with the Fermi surface nesting which exists in the normal state or arises after the superconducting transition. In view of the similarity of the incommensurability in yttrium and lanthanum cuprates this approach implies the near resemblance of their Fermi surfaces and their change with doping which is highly improbable. Besides, the applicability of the picture of itinerant electrons for underdoped cuprates casts doubts. As for the second notion, it should be noted that in the elastic neutron scattering the charge-density wave connected with stripes is observed only in crystals with the low-temperature tetragonal or the low-temperature less-orthorhombic phases ($\text{La}_{2-x}\text{Ba}_x\text{CuO}_4$ and $\text{La}_{2-y-x}\text{Nd}_y\text{Sr}_x\text{CuO}_4$) and does not observed in $\text{La}_{2-x}\text{Sr}_x\text{CuO}_4$ in the low-temperature orthorhombic phase [11]. At the same time the magnetic incommensurability is similar in these two types of crystals. It can be supposed that the magnetic incommensurability is the cause rather than the effect of stripes which are formed with an assistance of phonons.

In the present work the general formula for the magnetic susceptibility derived in the memory function approach [12] is used. For the description of spin excitations in the doped antiferromagnet the t - J model of a Cu-O plane is employed. In this approach the mentioned peculiarities of the magnetic properties of cuprates are reproduced including the proper frequency and momentum location of the susceptibility maxima. The incommensurability for $\omega > \omega_r$ is connected with the dispersion of spin excitations. The incommensurability for lower frequencies is related to the dip in the spin-excitation damping at \mathbf{Q} . For moderate doping this dip stems from the weakness of the interaction between the spin excitations and holes near the hot spots. Such form of the interaction constant follows from the fact that a decaying site spin excitation creates a fermion pair with components residing on the same and neighbor sites.

In the memory function approach the imaginary part of the magnetic susceptibility, which is directly connected with the cross-section of the magnetic

scattering, is described by the formula [13]

$$\chi''(\mathbf{k}\omega) = -\frac{4\mu_B^2\omega\Im R(\mathbf{k}\omega)}{[\omega^2 - \omega f_{\mathbf{k}}\Re R(\mathbf{k}\omega) - \omega_{\mathbf{k}}^2]^2 + [\omega f_{\mathbf{k}}\Im R(\mathbf{k}\omega)]^2}, \quad (1)$$

where $f_{\mathbf{k}} = (i\dot{s}_{\mathbf{k}}^z, -i\dot{s}_{-\mathbf{k}}^z)^{-1}$, $(A, B) = i\int_0^\infty dt\langle[A(t), B]\rangle$, the angular brackets denote the statistical averaging, $A(t) = e^{iHt}Ae^{-iHt}$ with the Hamiltonian H , μ_B is the Bohr magneton, $s_{\mathbf{k}}^z = N^{-1/2}\sum_{\mathbf{n}}e^{i\mathbf{k}\mathbf{n}}s_{\mathbf{n}}^z$ with the number of sites N and the z component of the spin $s_{\mathbf{n}}^z$ on the lattice site \mathbf{n} , $i\dot{s}_{\mathbf{k}}^z = [s_{\mathbf{k}}^z, H]$, $\omega_{\mathbf{k}}^2 = (i\dot{s}_{\mathbf{k}}^z, -i\dot{s}_{-\mathbf{k}}^z)(s_{\mathbf{k}}^z, s_{-\mathbf{k}}^z)^{-1}$, $R(\mathbf{k}\omega) = -i\int_0^\infty dt e^{i\omega t}(A_{2t}, A_2^\dagger)$ is the memory function with $A_2 = i^2\ddot{s}_{\mathbf{k}}^z - \omega_{\mathbf{k}}^2 s_{\mathbf{k}}^z$,

$$i\frac{d}{dt}A_{2t} = (1 - P_0)(1 - P_1)[A_{2t}, H], \quad A_{2,t=0} = A_2,$$

and the projection operators P_k , $k = 0, 1$, are defined as

$$P_k Q = (Q, A_k^\dagger)(A_k, A_k^\dagger)^{-1}A_k$$

with the operators $A_0 = s_{\mathbf{k}}^z$ and $A_1 = i\dot{s}_{\mathbf{k}}^z$.

To describe the spin excitations of Cu-O planes which determine the magnetic properties of cuprates the t - J model [14] is used. Its Hamiltonian reads

$$H = \sum_{\mathbf{n}\mathbf{m}\sigma} t_{\mathbf{n}\mathbf{m}} a_{\mathbf{n}\sigma}^\dagger a_{\mathbf{m}\sigma} + \frac{1}{2} \sum_{\mathbf{n}\mathbf{m}} J_{\mathbf{n}\mathbf{m}} \mathbf{s}_{\mathbf{n}} \mathbf{s}_{\mathbf{m}}, \quad (2)$$

where $a_{\mathbf{n}\sigma} = |\mathbf{n}\sigma\rangle\langle\mathbf{n}0|$ is the hole annihilation operator, \mathbf{n} and \mathbf{m} label sites of the square lattice, $\sigma = \pm 1$ is the spin projection, $|\mathbf{n}\sigma\rangle$ and $|\mathbf{n}0\rangle$ are site states corresponding to the absence and presence of a hole on the site, $s_{\mathbf{n}}^z = \frac{1}{2}\sum_{\sigma}\sigma|\mathbf{n}\sigma\rangle\langle\mathbf{n}\sigma|$ and $s_{\mathbf{n}}^\sigma = |\mathbf{n}\sigma\rangle\langle\mathbf{n}, -\sigma|$ are the spin- $\frac{1}{2}$ operators. Considering the interaction between nearest neighbor spins, described by the parameter J , and the hole hopping to nearest and next nearest neighbor sites, described by the parameters t and t' , respectively, the terms in Eq. (1) are brought to the form [13]

$$\begin{aligned} (i\dot{s}_{\mathbf{k}}^z, -i\dot{s}_{-\mathbf{k}}^z) &= 4(1 - \gamma_{\mathbf{k}})(J|C_1| + tF_1), \\ \omega_{\mathbf{k}}^2 &= 16J^2\alpha|C_1|(1 - \gamma_{\mathbf{k}})(\Delta + 1 + \gamma_{\mathbf{k}}), \\ \Im R(\mathbf{k}\omega) &= \frac{8\pi t\omega_{\mathbf{k}}^2}{N} \sum_{\mathbf{k}'} g_{\mathbf{k}\mathbf{k}'}^2 \int_{-\infty}^{\infty} d\omega' A(\mathbf{k}'\omega') \\ &\quad \times A(\mathbf{k} + \mathbf{k}', \omega + \omega') \frac{n_F(\omega + \omega') - n_F(\omega')}{\omega}, \end{aligned} \quad (3)$$

where $\gamma_{\mathbf{k}} = \frac{1}{2}[\cos(k_x) + \cos(k_y)]$, $C_1 = \langle s_{\mathbf{n}}^+ s_{\mathbf{n}+\mathbf{a}}^- \rangle$ and $F_1 = \langle a_{\mathbf{n}}^\dagger a_{\mathbf{n}+\mathbf{a}} \rangle$ are the spin and hole correlations on neighbor sites, \mathbf{a} is a vector connecting these sites, $\alpha \sim 1$ is the vertex correction parameter, $g_{\mathbf{k}\mathbf{k}'} = \gamma_{\mathbf{k}'} - \gamma_{\mathbf{k}+\mathbf{k}'} + \frac{t'}{t}(\gamma'_{\mathbf{k}'} - \gamma'_{\mathbf{k}+\mathbf{k}'})$, $\gamma'_{\mathbf{k}} = \cos(k_x) \cos(k_y)$, $n_F(\omega) = [\exp(\omega/T) + 1]^{-1}$ with the temperature T , $A(\mathbf{k}\omega)$ is the hole spectral function which is taken in the form

$$A(\mathbf{k}\omega) = \frac{\eta/\pi}{(\omega - \varepsilon_{\mathbf{k}} + \mu)^2 + \eta^2} \quad (4)$$

in this work. Here μ is the chemical potential, η is the artificial broadening, and $\varepsilon_{\mathbf{k}}$ is the hole dispersion.

In Eq. (3), $\Delta \propto \xi^{-2}$ where ξ is the correlation length of the short-range antiferromagnetic order [15]. Thus, in the short-range order the frequency of spin excitations at \mathbf{Q} is nonzero, in contrast to the classical antiferromagnetic magnons. As follows from Eq. (3), the dispersion of spin excitations has a local minimum at \mathbf{Q} and can be approximated as $\omega_{\mathbf{k}} = [\omega_{\mathbf{Q}}^2 + c^2(\mathbf{k} - \mathbf{Q})^2]^{1/2}$ near this momentum [13].

To simplify calculations let us set $T = 0$. Notice that $\Im R(\mathbf{k}\omega)$ is an even function of the frequency and consider the region $\omega \geq 0$. The integral in Eq. (3) reduces to $\int_{-\omega}^0 d\omega' A(\mathbf{k}'\omega')A(\mathbf{k} + \mathbf{k}', \omega + \omega')$ and for the spectral function (4) is easily integrated. For $\eta \ll \omega$ the states with energies $-\omega < \varepsilon_{\mathbf{k}'} - \mu < 0$ and $0 < \varepsilon_{\mathbf{k}+\mathbf{k}'} - \mu < \omega$ make the main contribution to this integral.

In the following, we use the values of C_1 , F_1 , Δ and α calculated self-consistently in the t - J model on a 20×20 lattice for the range of hole concentrations $0 \leq x \lesssim 0.16$ [15]. The calculations were carried out for the parameters $t = 0.5$ eV and $J = 0.1$ eV corresponding to hole-doped cuprates [16]. For $\varepsilon_{\mathbf{k}}$ we apply the hole dispersion $\varepsilon_{\mathbf{k}} = -0.0879 + 0.5547\gamma_{\mathbf{k}} - 0.1327\gamma'_{\mathbf{k}} - 0.0132\gamma_{2\mathbf{k}} + 0.0925[\cos(2k_x) \cos(k_y) + \cos(k_x) \cos(2k_y)] - 0.0265\gamma'_{2\mathbf{k}}$ proposed from the analysis of photoemission data in $\text{Bi}_2\text{Sr}_2\text{CaCu}_2\text{O}_8$ [17]. Here the coefficients are in electronvolts. Analogous results can be obtained also with other model dispersions [9,17].

The momentum dependence of $\chi''(\mathbf{k}\omega)$ calculated with the above equations is shown in Fig. 1. As seen from this figure, there are three frequency regions with different shapes of the momentum dependence of $\chi''(\mathbf{k}\omega)$. The first region is the vicinity of the frequency $\omega_{\mathbf{Q}}$ of the gap in the dispersion of spin excitations at \mathbf{Q} . For the parameters of Fig. 1 $\omega_{\mathbf{Q}} \approx 37$ meV. In this region χ'' is peaked at \mathbf{Q} . For smaller and larger frequencies the magnetic response is incommensurate. The dispersion of maxima in $\chi''(\mathbf{k}\omega)$ for scans along the edge and the diagonal of the Brillouin zone and their full widths at half maximum (FWHM) are shown in Fig. 2.

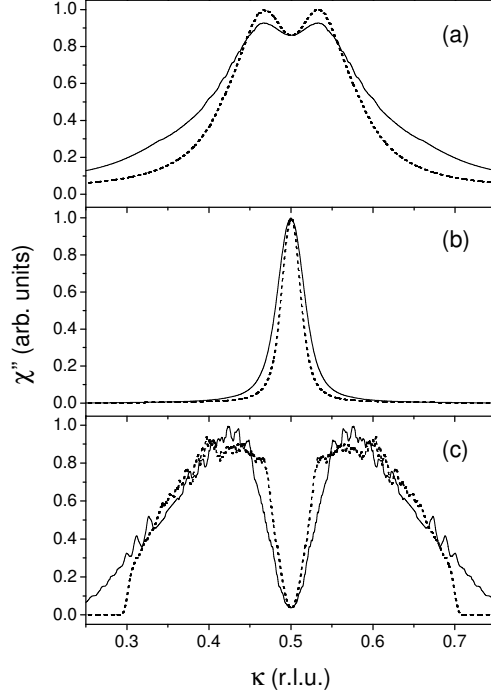


Fig. 1. Wave-vector scan of χ'' for $T = 0$, $x \approx 0.12$, $\mu = -40$ meV, and $\omega = 70$ meV, $\eta = 3.5$ meV (a), $\omega = 35$ meV, $\eta = 3.5$ meV (b), $\omega = 2$ meV, $\eta = 1.5$ meV (c). Calculations were carried out in a 1200×1200 lattice. The solid lines correspond to scans along the edge of the Brillouin zone, $\mathbf{k} = (\kappa, \frac{1}{2})$; the dashed lines are for the zone diagonal, $\mathbf{k} = (\kappa, \kappa)$.

To understand the above results notice that χ'' in Eq. (1) has the resonance denominator which will dominate in the momentum dependence for $\omega \geq \omega_{\mathbf{Q}}$ if the spin excitations are not overdamped. Parameters of Fig. 1 correspond to this case. For $\omega \geq \omega_{\mathbf{Q}}$ the equation $\omega = \omega_{\mathbf{k}}$ determines the positions of the maxima in $\chi''(\mathbf{k}\omega)$ which are somewhat shifted by the momentum dependence of $\Im R$ (for simplicity the term with $\Re R$ is included in $\omega_{\mathbf{k}}$). Using the above approximation for $\omega_{\mathbf{k}}$ we find that the maxima in χ'' are located near a circle centered at \mathbf{Q} with the radius $c^{-1}(\omega^2 - \omega_{\mathbf{Q}}^2)^{1/2}$ [13,18].

For $\omega < \omega_{\mathbf{Q}}$ the nature of incommensurability is completely different. It is most easily seen in the limit of small ω when Eq. (1) reduces to $\chi''(\mathbf{k}\omega) \propto \omega_{\mathbf{k}}^{-4} \Im R(\mathbf{k}\omega)$. $\omega_{\mathbf{k}}^{-4}$ is a decreasing function of the difference $\mathbf{k} - \mathbf{Q}$ which acts in favor of a commensurate peak. However, if $\Im R(\mathbf{k}\omega)$ has a pronounced dip at \mathbf{Q} incommensurate peaks arise. For small x the dip appears due to the nesting of the ellipses forming the Fermi surface with the wave vector \mathbf{Q} [19]. For larger x the mechanism of the dip formation is the following. For $\mathbf{k} = \mathbf{Q}$ and small ω hole states which make the main contribution to $\Im R$ are located near the hot spots (see the inset in Fig. 2). For these states the interaction constant $g_{\mathbf{Q}\mathbf{k}'}$ in Eq. (3) is small which leads to the smallness of $\Im R$. With moving away from \mathbf{Q} momenta of states contributing to the damping recede from the hot spots and $g_{\mathbf{k}\mathbf{k}'}$ and $\Im R$ grow. Thus, the damping has a dip at \mathbf{Q}

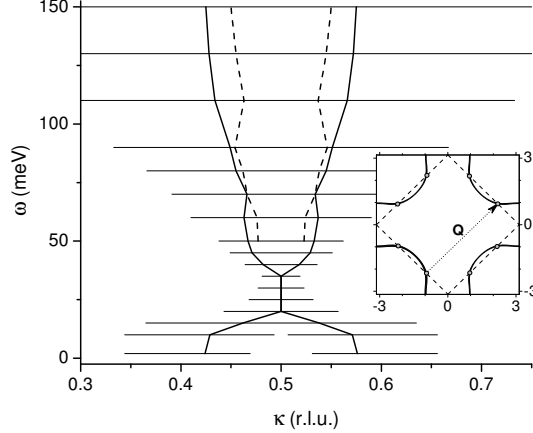


Fig. 2. The dispersion of maxima in $\chi''(\mathbf{k}\omega)$ for scans along the edge [$\mathbf{k} = (\kappa, \frac{1}{2})$, solid lines] and the diagonal [$\mathbf{k} = (\kappa, \kappa)$, dashed lines] of the Brillouin zone. The latter dispersion are drawn only in the frequency range in which these maxima are more intensive than those along the edge. Parameters are the same as in Fig. 1. Horizontal bars are FWHM for maxima along the edge. Inset: The Fermi surface for $\mu = -40$ meV (the solid line). Dashed lines show the boundary of the magnetic Brillouin zone, circles are the hot spots.

which leads to the low-frequency incommensurability shown in Fig. 1c. The smallness of $g_{\mathbf{Q}\mathbf{k}'}$ near the hot spots is related to the fact that the decaying site spin excitation creates the fermion pair on the same and neighbor sites. As a result $g_{\mathbf{k}\mathbf{k}'}$ contains the functions $\gamma_{\mathbf{k}'}$, $\gamma_{\mathbf{k}+\mathbf{k}'}$ and $\gamma'_{\mathbf{k}'} - \gamma'_{\mathbf{k}'+\mathbf{k}}$ vanishing on the boundary of the magnetic Brillouin zone and at $\mathbf{k} = \mathbf{Q}$.

The dispersion of peaks in χ'' which is similar to that shown in Fig. 2 was observed in $\text{YBa}_2\text{Cu}_3\text{O}_{7-y}$ and $\text{La}_{2-x}\text{Ba}_x\text{CuO}_4$ [4,8]. As seen from Fig. 1, for frequencies $\omega < \omega_{\mathbf{Q}}$ the susceptibility is peaked at $\mathbf{k} = (\frac{1}{2}, \frac{1}{2} \pm \delta)$ and $(\frac{1}{2} \pm \delta, \frac{1}{2})$, while for $\omega > \omega_{\mathbf{Q}}$ the maxima are located at $(\frac{1}{2} \pm \delta, \frac{1}{2} \pm \delta)$, $(\frac{1}{2} \pm \delta, \frac{1}{2} \mp \delta)$. This result is also in agreement with experimental observations [4,7,8]. Notice that in these crystals Fermi surfaces are similar to that shown in Fig. 2 [20]. The dependence of the incommensurability parameter δ on x for small ω is shown in Fig. 3. In agreement with experiment (see the inset in Fig. 3) δ grows nearly linearly with x up to $x \lesssim 0.12$ and then saturates. In these calculations the change of the hole dispersion with doping was not considered and the dependence $\delta(x)$ is connected solely with the variation of $\omega_{\mathbf{Q}} \propto \xi^{-1} \propto x^{1/2}$ [15]. We found that the low-frequency incommensurability disappears when $\eta > \omega$. Besides, it disappears also if μ approaches the extended van Hove singularities at $(0, \pi)$, $(\pi, 0)$. In this case for $\mathbf{k} = \mathbf{Q}$ the entire region of these singularities in which $g_{\mathbf{k}\mathbf{k}'}$ is nonzero contributes to $\Im R$. This may be the reason of the disappearance of the incommensurability in overdoped cuprates [2]. In the calculations the incommensurability disappears also in small lattices.

As mentioned above, for the parameters chosen spin excitations are not overdamped near \mathbf{Q} . As a consequence the frequency dependence of $\chi''(\mathbf{Q}\omega)$ has a

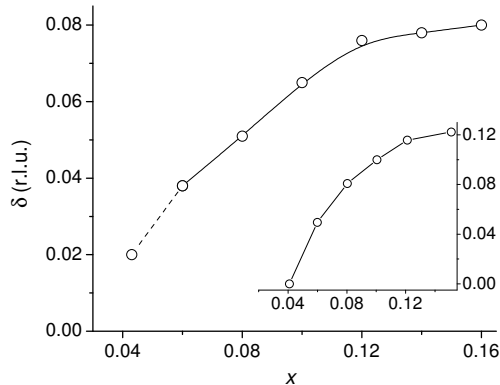


Fig. 3. The incommensurability parameter δ vs. x for $\omega = 2$ meV. The value of δ for $x = 0.043$ was taken from Ref. [19]. Inset: experimental data [2] for $\text{La}_{2-x}\text{Sr}_x\text{CuO}_4$. Connecting lines are a guide to the eye.

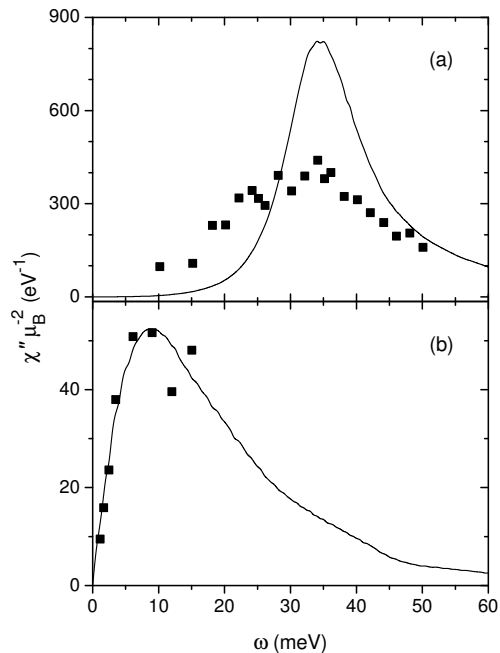


Fig. 4. The frequency dependence of χ'' . The solid lines are our results for $T = 0$, $x \approx 0.12$, $\mu = -40$ meV, $\eta = 3.5$ meV, $\mathbf{k} = \mathbf{Q}$ (a) and for $\mathbf{k} = (0.42, 0.5)$ and the scaled hole dispersion (see text) (b). Squares are the odd susceptibility in the normal-state $\text{YBa}_2\text{Cu}_3\text{O}_{6.83}$ ($x \approx 0.14$ [21]) at $T = 100$ K and $\mathbf{k} = \mathbf{Q}$ [5] (a) and the susceptibility in $\text{La}_{1.86}\text{Sr}_{0.14}\text{CuO}_4$ for $T = 35$ K at the incommensurate peak [6] (b).

pronounced maximum at $\omega \approx \omega_{\mathbf{Q}}$ which resembles the susceptibility observed in the superconducting and normal states of underdoped $\text{YBa}_2\text{Cu}_3\text{O}_{7-y}$. As seen in Fig. 4a, the experimental width of the maximum is approximately twice as large as the calculated one. Partly it is connected with the difference in temperatures for the two sets of the data. Besides, the decrease of the hole bandwidth and the increase of the hole damping lead to a substantial growth of $\Im R$ and to the overdamping of spin excitations [13]. An example

of such changes is shown in Fig. 4b where the results were obtained with the hole dispersion scaled by the factor 0.4. The calculations were carried out for $\mathbf{k} = (0.42, 0.5)$ which corresponds to the low-frequency incommensurate peak in Fig. 1c. The growth of $\Im R$ leads to the red shift of the maximum in $\chi''(\omega)$. Its position is no longer connected with the frequency of spin excitations. The similar frequency dependence of χ'' is observed in $\text{La}_{2-x}\text{Sr}_x\text{CuO}_4$ [6]. The increased $\Im R$ has no marked effect on the low-frequency incommensurability, however for the frequencies $\omega_{\mathbf{Q}} \geq \omega \geq 150$ meV we found only broad commensurate peaks for the parameters of Fig. 4b.

Our consideration was restricted to the normal state. Clearly the same mechanisms lead to the incommensurate magnetic response also in the superconducting state.

In summary, it was shown that the calculated momentum and frequency dependencies of the imaginary part of the susceptibility χ'' , the dispersion and location of maxima in it and the concentration dependence of the incommensurability parameter are similar to those observed in lanthanum and yttrium cuprates. The dispersion of the maxima in χ'' resembles two parabolas with upward and downward branches which converge at the antiferromagnetic wave vector \mathbf{Q} and at the respective frequency of spin excitations. We relate the upper parabola to the spin-excitation dispersion. The incommensurability connected with the lower parabola is related to the dip in the spin-excitation damping at \mathbf{Q} . For moderate doping the dip arises due to the smallness of the interaction between spin excitations and holes near the hot spots. In agreement with experiment the incommensurate peaks which form the lower parabola are located at momenta $(\frac{1}{2}, \frac{1}{2} \pm \delta)$, $(\frac{1}{2} \pm \delta, \frac{1}{2})$, while peaks in the upper parabola are at $(\frac{1}{2} \pm \delta, \frac{1}{2} \pm \delta)$, $(\frac{1}{2} \pm \delta, \frac{1}{2} \mp \delta)$. Also in agreement with experiment the low-frequency incommensurability parameter δ grows linearly with the hole concentration x for $x \lesssim 0.12$ and then saturates. By the variation of the hole bandwidth and damping the frequency dependencies of the susceptibility which resemble those observed in $\text{YBa}_2\text{Cu}_3\text{O}_{7-y}$ and $\text{La}_{2-x}\text{Sr}_x\text{CuO}_4$ were obtained.

This work was supported by the ESF grant No. 5548.

References

- [1] H. Yoshizawa, S. Mitsuda, H. Kitazawa, K. Katsumata, J. Phys. Soc. Jpn. 57 (1988) 3686.
- [2] K. Yamada, C. H. Lee, K. Kurahashi, J. Wada, S. Wakimoto, S. Ueki, H. Kimura, Y. Endoh, S. Hosoya, G. Shirane, R. J. Birgeneau, M. Greven, M. A. Kastner, Y. J. Kim, Phys. Rev. B 57 (1998) 6165.

- [3] T. E. Mason, G. Aeppli, S. M. Hayden, A. P. Ramirez, H. A. Mook, *Phys. Rev. Lett.* 71 (1993) 919.
- [4] P. Dai, H. A. Mook, F. Dogan, *Phys. Rev. Lett.* 80 (1998) 1738.
- [5] P. Bourges, in *The Gap Symmetry and Fluctuations in High Temperature Superconductors*, edited by J. Bok *et al.*, (Plenum Press, 1998), p. 349.
- [6] G. Aeppli, T. E. Mason, S. M. Hayden, H. A. Mook, J. Kulda, *Science* 279 (1997) 1432.
- [7] S. M. Hayden, H. A. Mook, P. Dai, T. G. Perring, F. Doğan, *Nature* 429 (2004) 531.
- [8] J. M. Tranquada, H. Woo, T. G. Perring, H. Goka, G. D. Gu, G. Xu, M. Fujita, K. Yamada, *Nature* 429 (2004) 534.
- [9] D. Z. Liu, Y. Zha, and K. Levin, *Phys. Rev. Lett.* 75 (1995) 4130; J. Brinckmann and P. A. Lee, *Phys. Rev. Lett.* 82 (1999) 2915.
- [10] V. Hizhnyakov, E. Sigmund, *Physica C* 156 (1988) 655; J. Zaanen, O. Gunnarsson, *Phys. Rev. B* 40 (1989) R7391.
- [11] H. Kimura, K. Hirota, H. Matsushita, K. Yamada, Y. Endoh, S.-H. Lee, C. F. Majkrzak, R. Erwin, G. Shirane, M. Greven, Y. S. Lee, M. A. Kastner, R. J. Birgeneau, *Phys. Rev. B* 59 (1999) 6517.
- [12] H. Mori, *Progr. Theor. Phys.* 34 (1965) 399.
- [13] A. Sherman, M. Schreiber, *Phys. Rev. B* 68 (2003) 094519.
- [14] Yu. A. Izyumov, *Usp. Fiz. Nauk* 167 (1997) 465 [*Phys.-Usp. (Russia)* 40 (1997) 445].
- [15] A. Sherman, M. Schreiber, *Eur. Phys. J. B* 32 (2003) 203.
- [16] V. A. Gavrichkov, S. G. Ovchinnikov, A. A. Borisov, E. G. Goryachev, *Zh. Eksp. Teor. Fiz.* 118 (2000) 422 [*JETP (Russia)* 91 (2000) 369].
- [17] M. R. Norman, *Phys. Rev. B* 61 (2000) 14751.
- [18] V. Barzykin, D. Pines, *Phys. Rev. B* 52 (1995) 13585.
- [19] A. Sherman, M. Schreiber, *Phys. Rev. B* 69 (2004) 100505(R).
- [20] A. Damascelli, Z. Hussain, Z.-X. Shen, *Rev. Mod. Phys.* 75 (2003) 473
- [21] J. L. Tallon, C. Bernhard, H. Shaked, R. L. Hitterman, and J. D. Jorgensen, *Phys. Rev. B* 51 (1995) R12911.